JOURNAL OF GEOPHYSICAL RESEARCH, VOL. 102, NO. D7, PAGES 8845–8854, APRIL 20, 1997

Refraction and atmospheric photochemistry

M. Balluch and D. J. Lary

Centre For Atmospheric Science, Cambridge University, U.K.

Abstract. A new model for calculating the effects of refraction is introduced. This model was invented independently of the one described by *DeMajistre et al.* [1995], but it is shown that the two models are analytically equivalent. However, the numerical implementation of the model introduced here is vastly more economical and efficient than that of the model by DeMajistre et al. This is because the two differential equations solved numerically by DeMajistre et al. have been solved analytically for the new model, prior to the numerical implementation, which reduced them to only one simple expression. The effects of refraction on stratospheric chemistry calculated with this new model are shown to be greatest in the polar lower stratosphere close to the onset and completion of polar night. The main effect is to change the shape of the seasonal cycle of reactive species produced by photolysis such as NO, NO_2, OH, HO_2, Cl, ClO, Br, and BrO during the onset and completion of polar night.

Introduction

Recent developments in measurements of photodissociation crosssections and photodissociation rates have stimulated further improvements of photochemical modeling. One such improvement has been the inclusion of effects of atmospheric refraction of the solar beam [*Anderson and Lloyd*, 1990]. Refraction is only important for large solar zenith angles. However, it is the polar springtime with its large solar zenith angles that has attracted much attention lately in connection with the formation of the so-called ozone hole. Therefore the effects of refraction on the photochemistry in the lower stratosphere merit a detailed investigation.

In the following, a new refraction model will be introduced, which is particularly suitable for use in the new radiation model described by *Balluch* [1996], but it can also be used in models with more commonly used coordinate systems. This new refraction model will be compared with another refraction model introduced independently by *DeMajistre et al.* [1995]. It will be shown that the model introduced here offers an improvement to the model by *DeMajistre et al.* [1995]. Although the two models are based on the same idea and are analytically equivalent, the model introduced here makes use of the coordinate system, which was introduced by *Balluch* [1996] for the radiation equation, to simplify the refraction equations considerably.

In the next section the new refraction model will be deduced and compared to that of *DeMajistre et al.* [1995]. Further, the effects of atmospheric refraction on lower stratospheric photochemistry, with particular emphasis on the onset and completion of the polar night, will be discussed.

Paper number 96JD03399.
0148-0227/97/96JD-03399$09.00

Refraction Model

In the following section the model for refraction as used for the calculations in this article will be described. This model was invented independently of the one described by *DeMajistre et al.* [1995]. It will be shown that the two models are actually analytically equivalent. To show this equivalence as well as to introduce the model mathematically in an easy to follow, deductive way, we will start our deduction with equation (6) from *DeMajistre et al.* [1995].

Basic Mathematics

DeMajistre et al. [1995] ended the derivation of their model with the following two equations

$$\frac{dy}{dx} = -\frac{\wp}{H} \tag{1}$$

$$\frac{d\wp}{dx} = -\left(\frac{\Psi}{H}\right)\frac{\partial \Psi}{\partial y} \tag{2}$$

These equations describe the bent solar beam as a function $y(x)$ in Cartesian coordinates. Here $\wp$ is the conjugate momentum to the generalized coordinate y, while x plays the role of the time in the Hamilton formalism. There is no z coordinate, since an incoming beam in the (x, y)-plane will not be bent out of this plane, because it was assumed that Ψ, the refractive index of the atmospheric air, is only a function of altitude. Hence the z coordinate dependency can be removed. The Hamilton function H is

$$H(x, y, \wp) = -\sqrt{\Psi^2 - \wp^2} \tag{3}$$

Equations (1) to (3) were derived by *DeMajistre et al.* [1995] by minimizing the time used by light traveling from one point to another and applying the Hamilton formalism to the problem. The authors then integrated these equations numerically to calculate the direct solar beam when bent by refraction, referred to as the bent solar beam in the following.

We want to proceed from this point by taking more advantage of the assumption that Ψ is a function of the distance to the center of the Earth, r, only, i.e., $\Psi = \Psi(r)$. For such a situation it might be advantageous to introduce polar coordinates (r, θ) instead of Cartesian coordinates (x, y) (see Figure 1). Let us also introduce the angle α as the angle between the tangent of the bent solar beam and the line through the center of the Earth, i.e., the center of the Cartesian coordinate system (Figure 1). This angle α is called the apparent solar zenith angle.

We can now represent the bent solar beam as $\alpha = \alpha(r)$. For that purpose, we need to transform the above equations into the new coordinate system (r, θ) and express the derivatives with respect to r as the time parameter along the bent solar beam. It is easy to prove that equation (2) becomes

$$\frac{d\wp}{dr} = -\frac{\Psi \tan\theta}{H - \wp \tan\theta} \frac{d\Psi}{dr} \tag{4}$$

From Figure 1 it is obvious that

$$\frac{dy}{dx} = \tan(\theta - \alpha) \tag{5}$$

With equation (1), this leads immediately to

$$\tan\theta = \frac{H \tan\alpha - \wp}{H + \wp \tan\alpha} \tag{6}$$

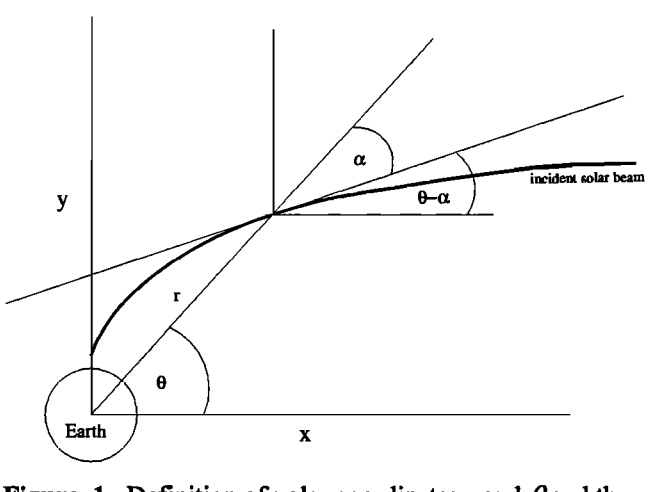

Figure 1. Definition of polar coordinates r and θ and the apparent solar zenith angle α. The size of the Earth and its atmosphere are totally out of proportion to make the definitions clearer.

and

$$\tan\alpha = \frac{\wp + H \tan\theta}{H - \wp \tan\theta} \tag{7}$$

Furthermore, with equations (1), (3), and (5), we can deduce

$$\wp = \Psi \sin(\theta - \alpha) \tag{8}$$

With equation (3) it immediately follows that the Hamilton function becomes

$$H = -\Psi \cos(\theta - \alpha) \tag{9}$$

Equations (4) and (8) are essentially the new equations (2) and (1), respectively. And equation (9) substitutes for equation (3). We can therefore proceed meaningfully by combining the two equations (4) and (8) by taking the derivative of equation (8) with respect to r and equating that to the righthand side of equation (4). With a bit of reshuffling and the use of equation (7), we arrive at

$$\frac{d(\theta - \alpha)}{dr} = \frac{1}{\Psi} \frac{d\Psi}{dr} \tan\alpha \tag{10}$$

This equation is remarkable because the dependency on $\wp$ of the lefthand side has disappeared, effectively reducing the original system of equations (1) and (2) to describe the bent solar beam, to only one equation (10) to describe the same bent solar beam. Next, considering that

$$\tan\theta = \frac{y}{x} \tag{11}$$

we can derive

$$\frac{d\theta}{dr} = -\frac{1}{r} \tan\alpha \tag{12}$$

With the help of that equation we can now write the equation for the bent solar beam $\alpha = \alpha(r)$:

$$\frac{d\alpha}{dr} = -\frac{1}{r} \tan\alpha - \frac{1}{\Psi} \frac{d\Psi}{dr} \tan\alpha \tag{13}$$

Balluch [1996] introduced a radiation model that uses a new coordinate system (r, p, q), which drastically simplifies the radiation equation. The coordinate q is defined as the tangent of the local azimuth of the line of sight times the cosine of α. In our application, for the direct solar beam, the azimuth is zero by definition, and therefore $q = 0$. The coordinate p is defined as

$$p = r \sin\alpha \tag{14}$$

From that we deduce

$$\frac{dp}{dr} = \sin\alpha + r \cos\alpha \frac{d\alpha}{dr} \tag{15}$$

and with the use of equation (12) the new equation describing the bent solar beam becomes

$$\frac{dp}{dr} = -\frac{p}{\Psi} \frac{d\Psi}{dr} \tag{16}$$

which would simply be obtainable from Snell's law as well.

This we can integrate analytically and arrive at

$$p(r) = p(r_{\text{out}}) \frac{\Psi(r_{\text{out}})}{\Psi(r)} \tag{17}$$

This is the new equation for the bent solar beam with refraction. Without additional assumptions we have reduced the system of differential equations, equations (1) and (2) as used by *DeMajistre et al.* [1995], to a very simple expression, equation (17), describing exactly the same thing.

Let us assume that the atmosphere is represented by a number of discrete spherical shells of constant physical properties like density and temperature (and therefore refractive index Ψ as well), as it would be in a numerical model. At each interface between the layers we could apply Snell's law to calculate refraction. Let's give the outside a superscript 'plus' and the inside a superscript 'minus'. Then we have in our terminology

$$\frac{p^+}{p^-} = \frac{\sin\alpha^+}{\sin\alpha^-} = \frac{\Psi^-}{\Psi^+} \tag{18}$$

If we consider now that the atmosphere consists of a number of such shells and interfaces between them, we arrive exactly at equation (17). In contrast to what appears to be a claim of *DeMajistre et al.* [1995] (at the beginning of the section 2: Refraction Model), the Hamiltonian approach and Snell's law are exactly the same in the discrete representation.

As can be seen in Figure 2, the bent solar beam is now represented by steps of decreasing p values. To calculate the optical depth τ, we have only to add the width of each of these "p steps" times the extinction per length, σ:

$$\Delta_{i,i+1}\tau = \left(\sqrt{r_i^2 - p_{i,i+1}^2} - \sqrt{r_{i+1}^2 - p_{i,i+1}^2}\right) \sigma_{i,i+1} \tag{19}$$

where $\sigma_{i,i+1}$ is the average value of σ between radius r_i and radius r_{i+1}.

Method of Solution

According to Figure 1, $\alpha(r)$ is the apparent solar zenith angle at r. We still need to set this in relation to the true solar zenith angle β, which is the angle between the solar beam and the zenith if there was no refraction, i.e., if the solar beam was a straight line. The basic observation to start from is that for each shell $(i, i+1)$, i.e., on any straight line, β changes exactly as α,

$$\beta_{i+1} - \beta_i = \alpha_{i+1}^+ - \alpha_i^- \tag{20}$$

where α_i^+ is the outer value of α at interface r_i and α_i^- is the inner value of α at interface r_i. Over each interface i, however, only α changes, according to equation (18). Consequently, we can add up equation (20), and since $\alpha_{\text{out}} = \beta_{\text{out}}$ outside the outermost shell, we arrive at

$$\beta_j = \alpha_{\text{out}} + \sum_{i=1}^{j-1} (\alpha_{i+1}^+ - \alpha_i^-) \tag{21}$$

That means for a given value of α_{out}, we can calculate a true solar zenith angle β_j at any radius r_j. In practical applications we will only know β_j and want to calculate α_{out} in order to use equations (17) and (19) for solving the radiation problem. For that we have to solve equation (21) for α_{out} with a shooting procedure. For this shooting procedure we use a first guess for α_{out} and then integrate equation (21) to yield a β_j, which we can compare to the true solar zenith angle we want to achieve. Depending on whether the solution β_j of equation (21) with our guess for α_{out} is larger or smaller than the true solar zenith angle we want to reach, we choose a better guess for α_{out}, larger or smaller than the former, to yield a better solution β_j of equation (21). This procedure we repeat iteratively until β_j and the true solar zenith angle we want to achieve agree to sufficient accuracy. For the first guess, we could choose α_{out}, as it would be without refraction. This shooting procedure becomes necessary because all α values depend on the outermost α, i.e., α_{out}, according to equation (17).

There are, however, a few more problems to consider. The above is strictly true only for solar zenith angles β_j, where the bent solar beam hits r_j directly, without passing first through a tangent point in the atmosphere, i.e., a point of closest proximity to the Earth, before reaching the altitude of interest. Also, for certain β_j, r_j might actually lie in the shadow of the Earth, i.e.,not in direct sunlight.

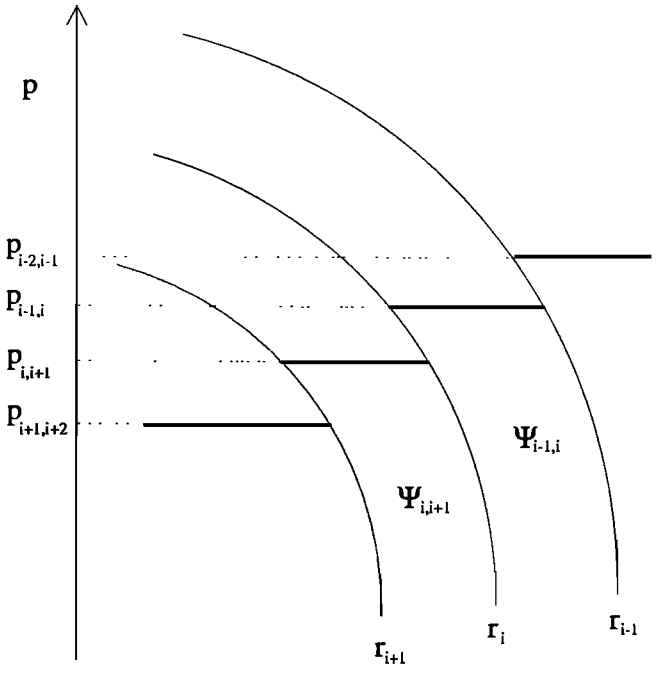

Figure 2. The bent solar beam in discrete approximation in coordinates r and p is represented by steps of constant p values (thick line segments). Over the shell interfaces the refractive indices change discontinuously. The p values change correspondingly, according to Snell's law (see equation [17] or [18]).

We can calculate the true solar zenith angle for both cases. For calculating the edge of the Earth's shadow, i.e., the terminator, we only need to calculate the bent solar beam that just about grazes on the surface of the Earth, i.e., the bent solar beam which has a tangent point at zero altitude. For calculating the bent solar beams which have a tangent point altitude of exactly the altitude of interest, i.e.,those bent solar beams that end tangentially for each r_j, we only have to solve equation (21) for $\alpha_j^+ = 90°$. All these cases of calculating bent solar beams with tangent points at given altitudes can be solved directly with only one integration of equation (21). It is easy to show that the true solar zenith angle for the case of $\alpha_j^+ = 90°$ at r_j is

$$\beta_j^{dmax} = \alpha_{out} + \sum_{i=1}^{j-1} \left(\arcsin\left(\frac{r_j \Psi_{j-1,j}}{r_{i+1} \Psi_{i,i+1}} \right) - \arcsin\left(\frac{r_j \Psi_{j-1,j}}{r_i \Psi_{i,i+1}} \right) \right) \quad (22)$$

For all j such that $\beta_j > \beta_j^{dmax}$, the solar beam will pass its tangent point. For all j such that $\beta_j < \beta_j^{dmax}$, the solar beam will not have a tangent point at all. This is important because if there is a tangent point, equation (21) does not really apply. However, since the solar beam is symmetric with regard to the tangent point, for the cases with a tangent point, we have to add those p steps on the other side of the tangent point twice in the sum of equation (21). In that way we can calculate the true solar zenith angle for the terminator

$$\beta_j^{max} = \alpha_{out} + \sum_{i=1}^{j-1} \left(\arcsin\left(\frac{r_N \Psi_{N-1,N}}{r_{i+1} \Psi_{i,i+1}} \right) - \arcsin\left(\frac{r_N \Psi_{N-1,N}}{r_i \Psi_{i,i+1}} \right) \right) + 2 \sum_{i=j}^{N-1} \left(\arcsin\left(\frac{r_N \Psi_{N-1,N}}{r_{i+1} \Psi_{i,i+1}} \right) - \arcsin\left(\frac{r_N \Psi_{N-1,N}}{r_i \Psi_{i,i+1}} \right) \right) \quad (23)$$

where N is the largest index, i.e.,r_N is the surface of the Earth. For all j such that $\beta_j > \beta_j^{max}$, r_j is in the shadow of the Earth, i.e.,not in direct sunlight. For all j such that $\beta_j < \beta_j^{max}$, r_j is in direct sunlight.

What remains to be shown is that α_{out} is actually a monotonic function of β, so that the shooting procedure converges, i.e., that we can guess from the error in β to a better boundary value α_{out} in an efficient and deterministic way. Figure 3 shows the relation of β and α_{out} with and without refraction for a typical midlatitude profile at an altitude of 20 km and a wavelength of 400 nm. The turning point of the curve is exactly at $\beta = \beta^{dmax}$. We can see that if we split the problem into one with $\beta > \beta^{dmax}$ and $\beta < \beta^{dmax}$, as it is possible with the help of equation (22), we indeed have a monotonic relationship between β and α_{out} for each case separately.

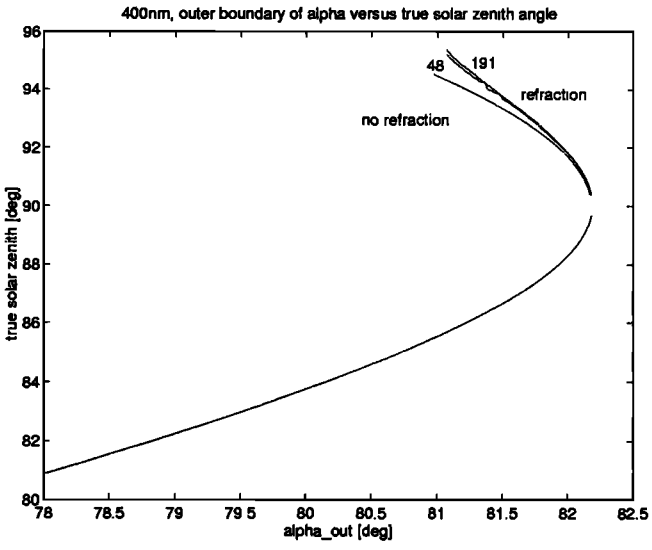

Figure 3. The true solar zenith angle β as a function of α_{out} for an altitude of 20 km and a wavelength of 400 nm. The lower branch corresponds to solar beams without tangent points, the upper branch to solar beams with tangent points. The changes of the upper branch are shown for with or without refraction, and for 48 or 191 spherical shells in the calculation with refraction.

In Figure 3 we can also see the difference with and without refraction. The two slightly different curves for the case with refraction are derived with 191 and 48 discrete spherical shells, as indicated in the Figure. As can be seen on the curves with realistic refractive index (realistic refractive index for air from *Birch and Downs* [1995]), the monotonicity can only be assured above a certain scale, depending on the number N of shells in the calculation. Even for 16 shells, though, the error in α_{out} is below $5 \times 10^{-4}\beta$.

Figure 4 shows the difference between apparent and true solar zenith angle at a wavelength of 175 nm. The difference increases to more than 1.3°. However, for a solar zenith angle below 85°, the difference is less than 0.2°. The enveloping of the contour lines at the largest true solar zenith angles gives the terminator.

The radiation model used for the results shown in the next section is the one from *Balluch* [1996] coupled with this refraction model. It should also be noted that the extension of this model for refraction from only applying to the direct solar beam to applying to all scattered and reflected beams is straightforward as long as all scattering processes are isotropic. All beams defined by constant p values would just have to be exchanged to p step functions as in Figure 2. However, for anisotropic scattering the dependency of the refraction equations on

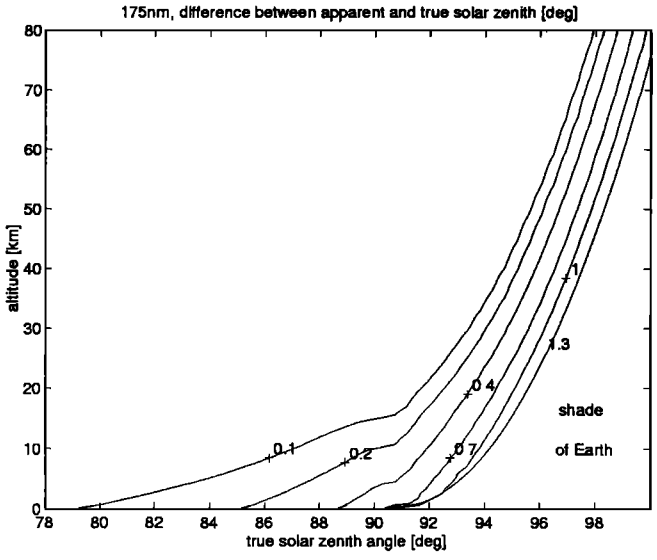

Figure 4. The difference between apparent and true solar zenith angle for a wavelength of 175 nm. The rightmost curve represents approximately the terminator with refraction, which is 1.3° further to the right than the terminator without refraction would be.

the β coordinate, as discussed above, cannot be removed so easily.

The method outlined can also be used with more commonly used coordinate systems for the radiative transfer equation, e.g., optical depth and polar and azimuthal angle. This may be achieved by calculating the optical depth with the help of equation (19).

Impact on Photochemistry

Refraction has its greatest effect on stratospheric chemistry in the polar lower stratosphere. In order to asses the impact of refraction alone on the chemistry of the lower stratosphere, a set of chemical box model calculations was perfomed. These simulations were for 50 mb (20 km) at a range of latitudes between 70° and 85°. The simulations started in autumn and went through to the following spring. The temperature was artificially kept at 205 K, so that the variations in the chemistry would be due to the motion of the Earth relative to the Sun alone.

Photochemical Model Description

The numerical model used was the AUTOCHEM model described by *Lary et al.* [1995, 1996], *Lary* [1996] and *Fisher and Lary* [1995]. The version of the model used in this study contains a total of 81 species. Of these, 74 species are integrated, namely; $O(^1D)$, $O(^3P)$, O_3, N, NO, NO_2, NO_3, N_2O_5, HONO, HNO_3, HO_2NO_2, CN, NCO, HCN, Cl, Cl_2, ClO, ClOO, OClO, Cl_2O_2, $ClNO_2$, $ClONO_2$, HCl, HOCl, CH_3OCl, Br, Br_2, BrO, $BrONO_2$, BrONO, HBr, HOBr, MeOBr, BrCl, H_2, H, OH, HO_2, H_2O_2, CH_3, CH_3O, CH_3O_2, CH_3OOH, CH_3ONO_2, $CH_3O_2NO_2$, HCO, HCHO, CF_3, CF_3O, CF_3O_2, CF_3OOCl, CF_3OH, CF_3OOH, CF_3OONO_2, F, F_2, FO, FO_2, F_2O_2, COF_2, FCO, FCOO, FCOOH, $FC(O)O_2$, FNO, FONO, FO_2NO_2, HF, CH_4, CHF_3, CH_3Br, CF_2Cl_2, N_2O, CO. The remaining seven species are not integrated and not in photochemical equilibrium, namely: CO_2, H_2O, O_2, N_2, $HCl_{(S)}$, $H_2O_{(S)}$, $HNO_{3(S)}$. The model contains a total of 438 reactions, 287 bimolecular reactions, 43 trimolecular reactions, 65 photolysis processes, and 43 heterogeneous reactions.

Refraction acts to extend the time per day for which light is present. As a result, when refraction is included in a numerical simulation we generally have higher concentrations of those species which are produced by photolysis.

The following sections will consider, in turn, the effect of refraction on various chemical species. The time period when refraction has the biggest effect is close to the onset and completion of polar night. However, the effects of refraction are also visible at much lower latitudes.

O_3

The effect of refraction on the ozone concentration is relatively small below 45 km. When refraction is included, the abundance of shortlived species such as Cl, Br, OH, and NO are increased, particularly close to the polar night boundary. This is because the period of time for which photolysis occurs is extended. As a result, when refraction was included, the ozone loss increased below 45 km, reaching a maximum additional loss of -0.5% over 7 days at around 40 km between 56° and 64° latitude. Figure 5 shows the percentage change in O_3 over 7 days due to refraction as a function of altitude and latitude at the solstice. The additional loss is not restricted to the region close to the polar night boundary but also extends into the tropics. Above approximately 48 km there is an increase in O_3 production due to increased photolysis, reaching a peak of approximately 10% at 65° latitude. Figure 5 shows that the high-latitude boundary of the region affected by refraction mirrors the polar night boundary, which moves poleward with increasing altitude.

Nitrogen Species

As can be seen in Figure 6, the enhancement in the NO and NO_2 concentration is significant (and lasts for several days) close to the polar night boundary. However, small changes also extend well into mid-latitudes. The region of increase in NO on the day side of the polar night boundary, which is greater than 10%, is considerable and extends over a few degrees of latitude centered on approximately 66° between 10 and 30 km. A similar response is observed for NO_2.

After polar night at a latitude of 70° the enhancement in NO_x is greater than 10% for a few weeks. The NO_x enhancement during polar night itself is not very signif-

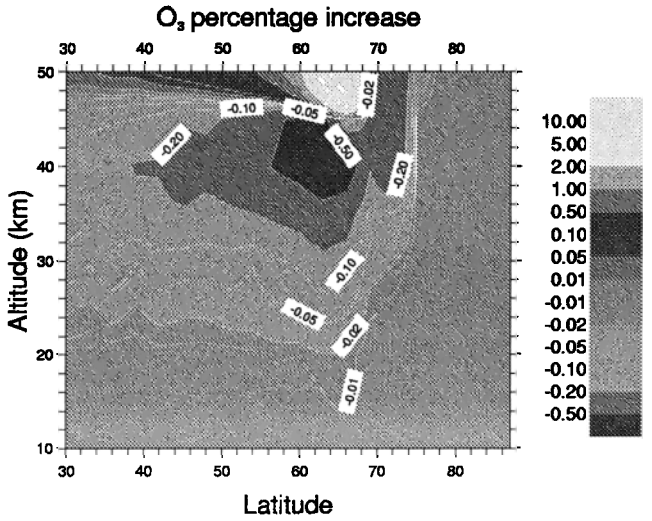

Figure 5. The percentage change in O_3 over 7 days due to refraction as a function of altitude and latitude at the solstice.

icant as during this period the NO_x concentrations are negligible. The effect of refraction on the HNO_3 concentration is small and restricted mainly to the upper stratosphere and mesosphere.

As the production of HONO is mainly due to the reaction of OH with NO, there is a considerable enhancement in the HONO concentration. The same is true for HO_2NO_2 which is produced by the reaction of HO_2 with NO_2.

Hydrogen Species

As can be seen in Figure 7, the enhancement in the H, OH, HO_2, CH_3 and HCHO concentration is significant and lasts for several days close to the onset and completion of polar night. The region of increase in H, OH, HO_2, CH_3 and HCHO extends over a few degrees of latitude centered on approximately 66° and occurs throughout the stratosphere. Refraction has slightly enhanced methane oxidation.

In the case of H_2O_2, an enhancement in HO_x caused by photolysis produces more H_2O_2, but in turn, H_2O_2 is also photolyzed. This generally results in a net reduction in H_2O_2.

Chlorine Species

As can be seen in Figure 8, the enhancement in the Cl and ClO concentration is significant and lasts for several days close to the onset and completion of polar night. At a latitude of 70° the enhancement in Cl lasts for about a month. The region of increase in Cl and ClO extends over a few degrees of latitude centered on approximately 66° and occurs throughout the stratosphere. In the lower stratosphere close to the polar night boundary the increase in ClO leads to a noticeable increase in Cl_2O_2 of up to 20%. However, at lower latitudes, due to its rapid photolysis including refraction reduces the Cl_2O_2 concentration.

Owing to the very rapid photolysis of HOCl, including refraction reduces the HOCl concentration in the lower stratosphere. In the upper stratosphere the increased abundance of HO_x and ClO_x means that the enhanced production of HOCl outweighs its enhanced photolysis and there is a net increase in HOCl.

In the lower stratosphere close to the polar night boundary the increased abundance of NO_2 and ClO due to refraction leads to an enhanced $ClONO_2$ concentration. This enhancement is most noticeable in the recovery period in early spring. However, above about 20 km the enhanced photolysis of $ClONO_2$ leads to a net reduction in its concentration, an effect which extends to much lower latitudes.

The effect of refraction on the HCl concentration is small.

Bromine Species

As can be seen in Figure 9, the enhancement in the Br and BrO concentration is significant (and lasts for several days) close to the onset and completion of polar night. It is an enhancement that extends throughout the stratosphere close to the polar night boundary.

Owing to its very rapid photolysis, including refraction reduces the concentration of BrCl. Also owing to its very rapid photolysis, including refraction reduces the HOBr concentration for several days close to the onset and completion of polar night. However, during the polar night itself the HOBr concentration is increased. This is a reflection of the increased HO_2 and BrO concentrations.

The increased abundance of NO_2 and BrO due to refraction leads to a considerable enhancement of the $BrONO_2$ concentration (of up to 20% and more). This enhancement is most noticeable in the recovery period in early spring.

The two main sources of HBr are the reactions of Br with HO_2 and HCHO. The increases in the Br and HO_2 concentrations therefore lead to an increase in the HBr concentration when refraction is included.

Summary

A new model for calculating the effects of refraction has been introduced. This model was invented independently of the one described by *DeMajistre et al.* [1995], but it is shown that the two models are analytically equivalent. However, the two differential equations that were solved numerically by *DeMajistre et al.* [1995] are solved analytically here to yield a vastly simplified analytical expression. It is this simplified expression which is numerically implemented in the model introduced here.

The effects of refraction on stratospheric chemistry have been considered and are shown to be greatest in

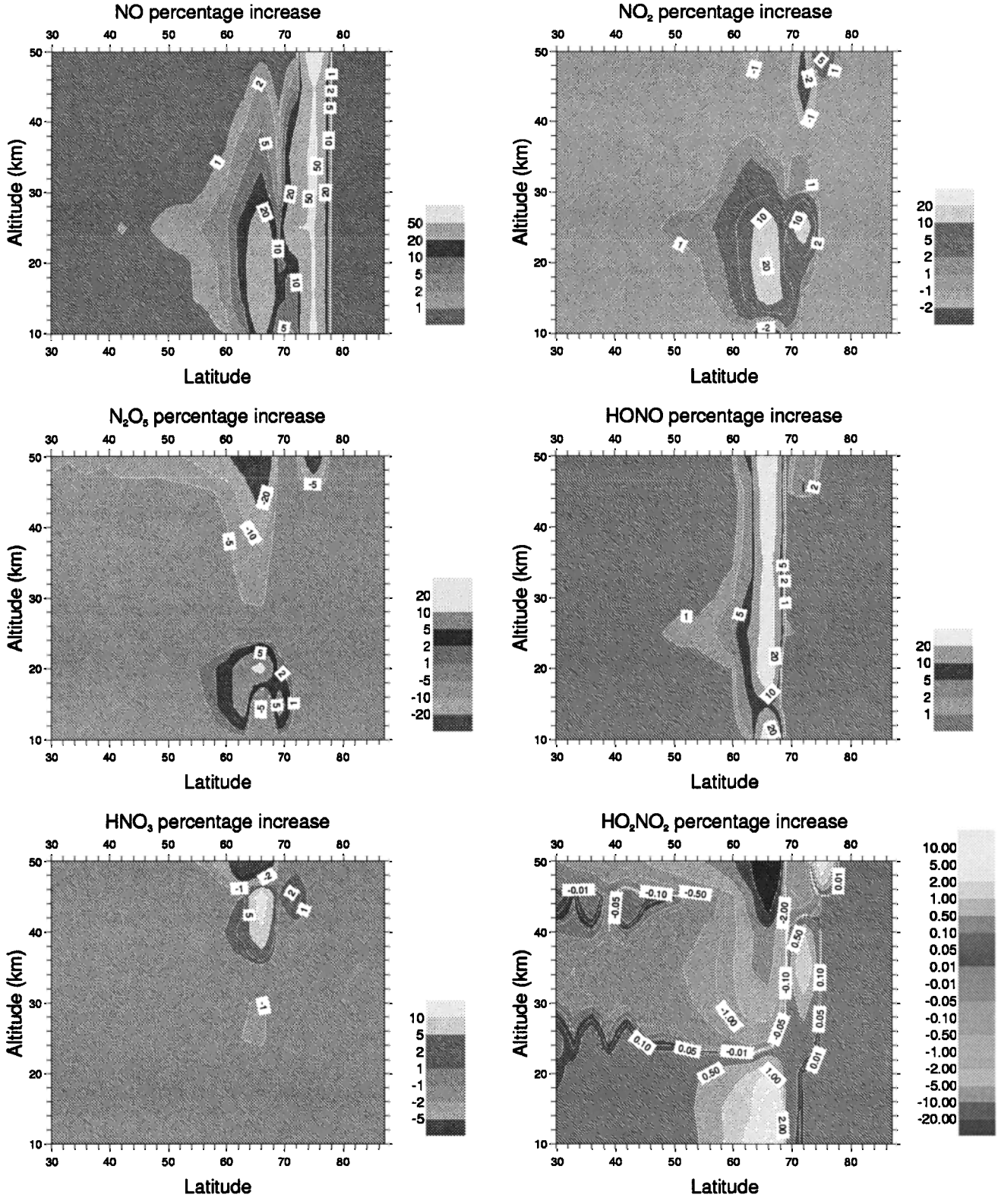

Figure 6. The percentage change in noon NO, NO_2, N_2O_5, HONO, HNO_3 and HO_2NO_2 over 7 days due to refraction as a function of altitude and latitude at the solstice.

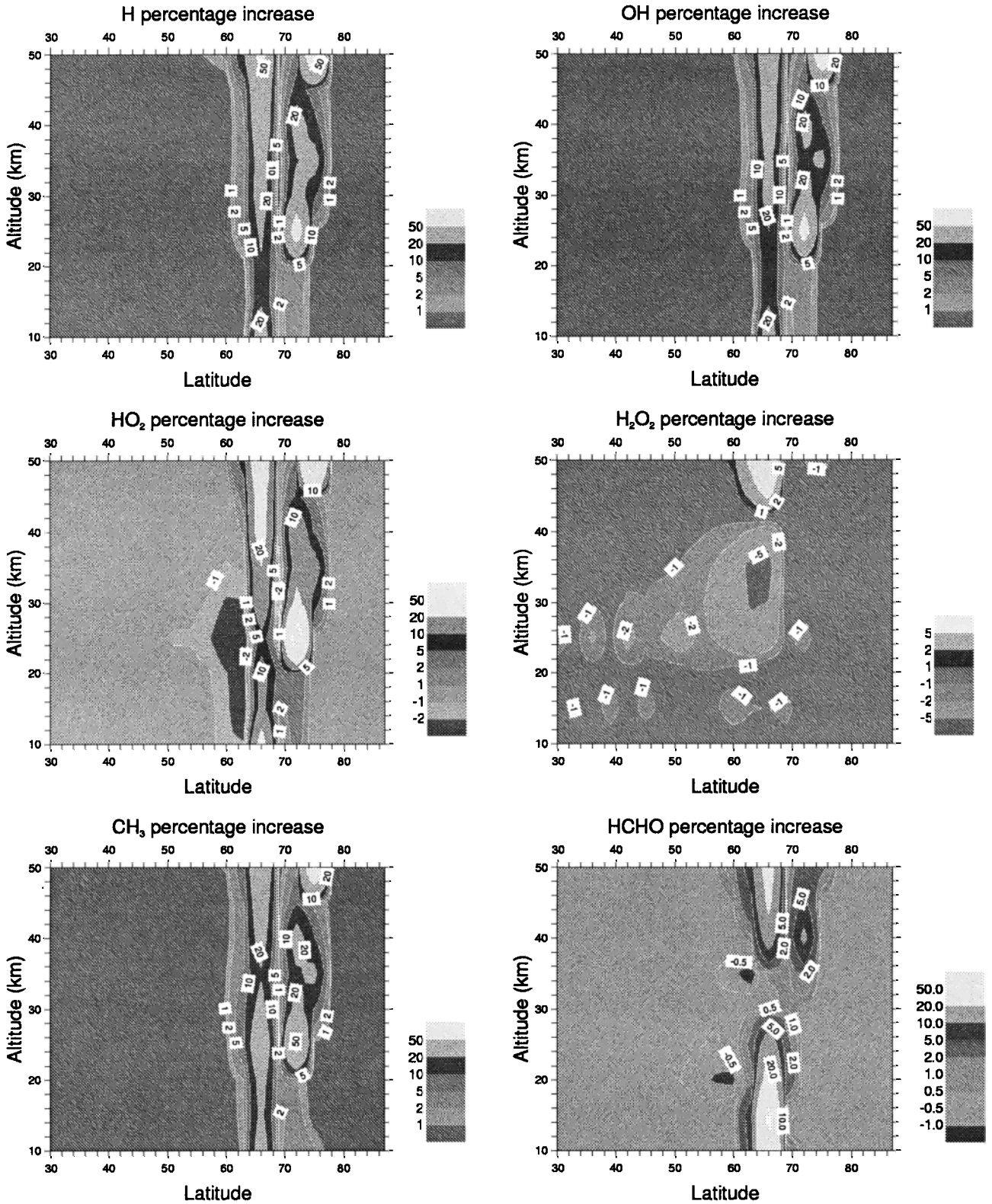

Figure 7. The percentage change in noon H, OH, HO_2, H_2O_2, CH_3 and HCHO over 7 days due to refraction as a function of altitude and latitude at the solstice.

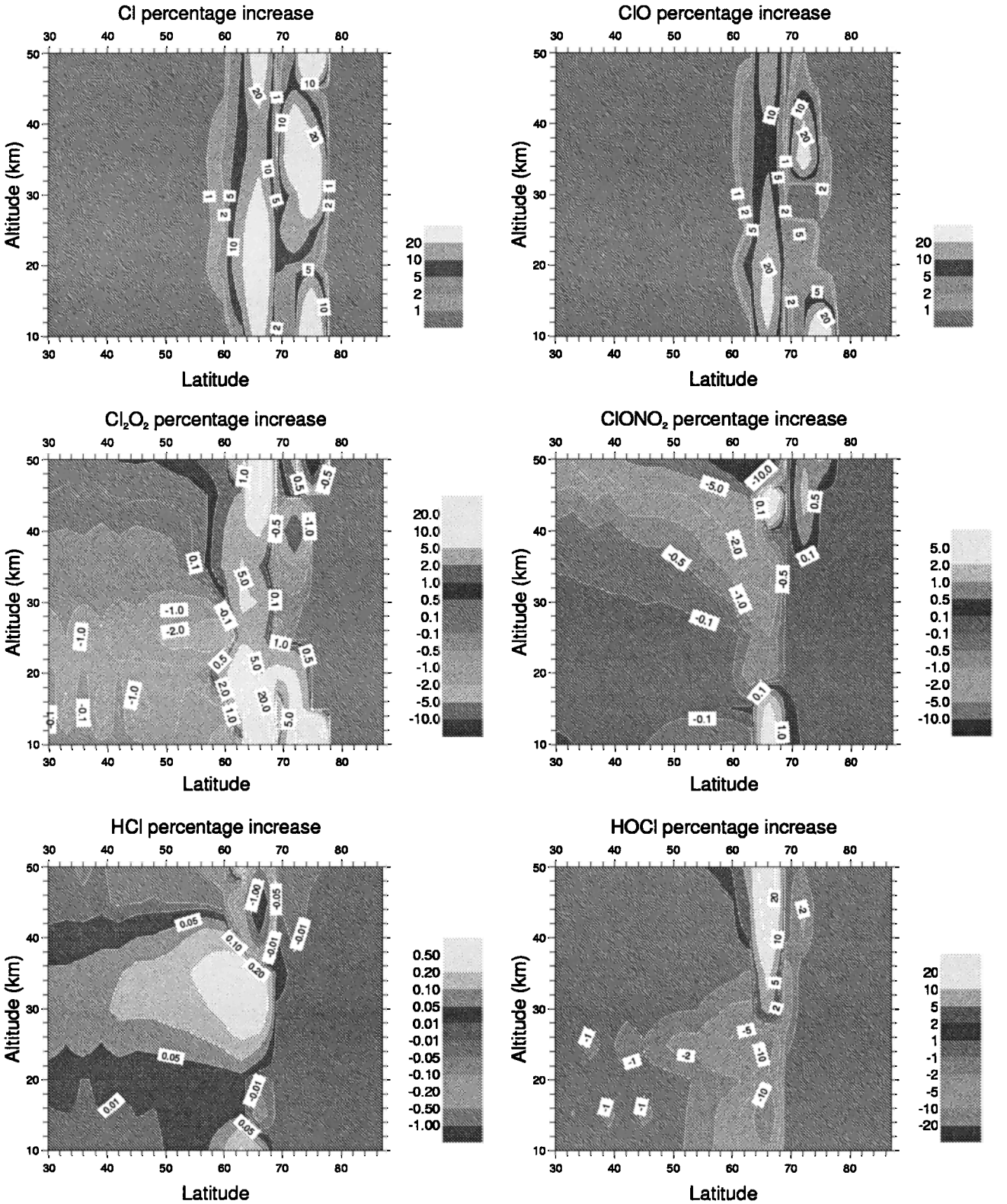

Figure 8. The percentage change in noon Cl, ClO, Cl_2O_2, $ClONO_2$, HCl and HOCl over 7 days due to refraction as a function of altitude and latitude at the solstice.

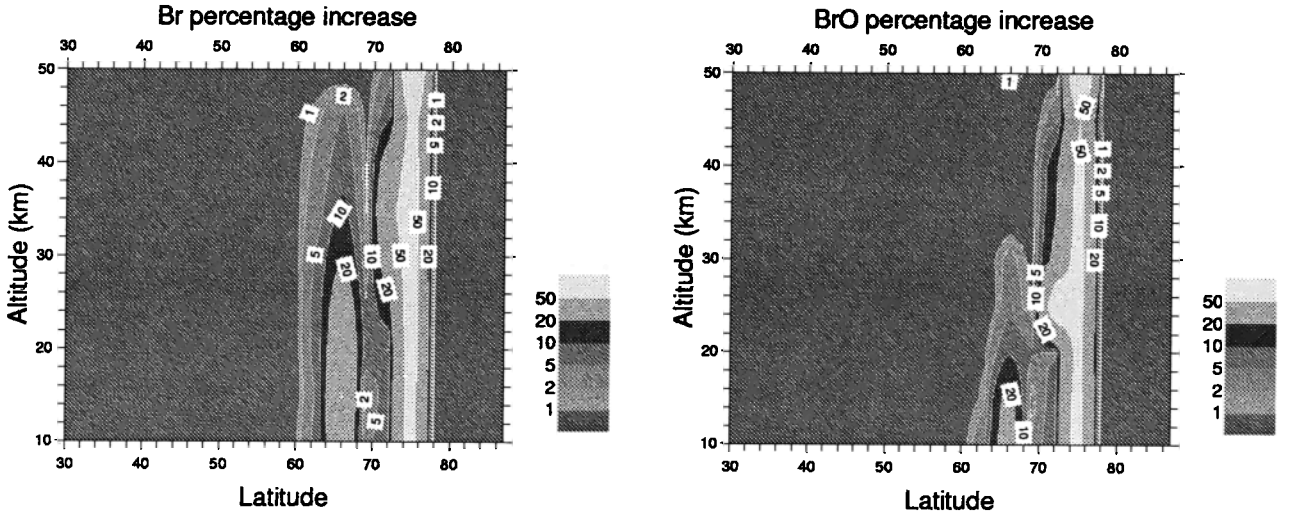

Figure 9. The percentage change in noon Br, BrO, HOBr and $BrONO_2$ over 7 days due to refraction as a function of altitude and latitude at the solstice.

the region close to the polar night boundary. During this period the concentration of species produced by photolysis, such as OH, NO, Cl and Br, are considerably enhanced. In the simulations presented here the effect on ozone depletion due to the inclusion of refraction was up to 0.5% over a 7-day period between two simulations, one which included refraction and one which did not include refraction. The ozone loss was not restricted to the region close to the polar night boundary but also extended to low latitudes. If, however, there are large regions of cold temperatures during the onset and completion of polar night the additional ozone depletion could be larger than the results presented here.

In contrast, in the upper stratosphere and lower mesosphere, increased photolysis leads to a considerable enhancement in the O_3 concentration.

The main effect of refraction is to change the shape of the seasonal cycle of reactive species produced by photolysis such as NO, NO_2, OH, HO_2, Cl, ClO, Br, and BrO during the onset and completion of polar night.

Acknowledgments. David Lary is a Royal Society University Research Fellow and wishes to thank the Royal Society for its support and J.A. Pyle for his helpful cooperation. The Centre for Atmospheric Science is a joint initiative of the Department of Chemistry and the Department of Applied Mathematics and Theoretical Physics. This work forms part of the NERC U.K. Universities Global Atmospheric modeling Programme.

References

Anderson, D. E., Jr., and S. A. Lloyd, Polar twilight UV-visible radiation field: Perturbations due to multiple scattering, ozone depletion, stratospheric clouds, and surface albedo, *J. Geophys. Res.*, *95*(D6), 7429-7434, 1990.

Balluch, M., A new numerical model to compute photolysis rates and solar heating with anisotropic scattering in spherical geometry, *Ann. Geophys.*, *14*, 80-97, 1996.

DeMajistre, R., D. E. Anderson, S. Lloyd, P. K. Swaminathan, and S. Zasadil, Effects of refraction on photochemical calculations, *J. Geophys. Res.*, *100*(D9), 18,817-18,822, 1995.

Fisher, M., and D. J. Lary, Lagrangian four dimensional variational data assimilation of chemical species, *Q. J. R. Meteorol. Soc.*, *121*(527) Part A, 1681-1704, 1995.

Lary, D. J., Gas phase atmospheric bromine photochemistry, *J. Geophys. Res.*, *101*(D1), 1505-1516, 1996.

Lary, D. J., M. P. Chipperfield, and R. Toumi, The potential impact of the reaction $OH+ClO \rightarrow HCl+O_2$ on polar ozone photochemistry, *J. Atmos. Chem.*, *21*(1), 61-79, 1995.

Lary, D. J., M. P. Chipperfield, R. Toumi and T. M. Lenton, Atmospheric heterogeneous bromine chemistry, *J. Geophys. Res.*, *101*(D1), 1489-1504, 1996.

M. Balluch, Centre For Atmospheric Science, Department of Applied Maths and Theoretical Physics, Cambridge University, Silver Street, Cambridge, England. (e-mail: mgb@damtp.cam.ac.uk)

D. J. Lary Centre For Atmospheric Science, Department of Chemistry, Cambridge University, Lensfield Road, Cambridge, CB2 1EW, England. (e-mail: david@atm.ch.cam.ac.uk)

(Received April 18, 1996; revised October 11, 1996; accepted October 11, 1996.)